ELSEVIER

Biochemical Pharmacology 63 (2002) 2121–2136

Biochemical Pharmacology

A critical role for a tyrosine residue in the cannabinoid receptors for ligand recognition

Sean D. McAllister[a], Qing Tao[b], Judy Barnett-Norris[c], Kurt Buehner[c], Dow P. Hurst[c], Frank Guarnieri[d], Patricia H. Reggio[c], Katharine W. Nowell Harmon[e], Guy A. Cabral[e], Mary E. Abood[a,*]

[a]*Forbes Norris ALS/MDA Research Center, California Pacific Medical Center, 2351 Clay St., Suite 416, San Francisco, CA 94115, USA*
[b]*Department of Pharmacology and Toxicology, Virginia Commonwealth University, Richmond, VA 23298, USA*
[c]*Chemistry Department, Kennesaw State University, Kennesaw, GA 30144, USA*
[d]*Physiology and Biophysics Department, Mt. Sinai School of Medicine, New York, NY 10029, USA*
[e]*Department of Microbiology and Immunology, Virginia Commonwealth University, Richmond, VA 23298, USA*

Received 5 January 2001; accepted 17 December 2001

Abstract

Previous mutation and modeling studies have identified an aromatic cluster in the transmembrane helix (TMH) 3-4-5 region as important for ligand binding at the CB_1 and CB_2 cannabinoid receptors. Through novel mixed mode Monte Carlo/Stochastic Dynamics (MC/SD) calculations, we tested the importance of aromaticity at position 5.39(275) in CB_1. MC/SD calculations were performed on wild-type (WT) CB_1 and two mutants, Y5.39(275)F and Y5.39(275)I. Results indicated that while the CB_1 Y5.39(275)F mutant is very similar to WT, the Y5.39(275)I mutant shows pronounced topology changes in the TMH 3-4-5 region. Site-directed mutagenesis studies of tyrosine 5.39 to phenylalanine (Y → F) or isoleucine (Y → I) in both CB_1 and CB_2 were performed to determine the functional role of this amino acid in each receptor subtype. HEK 293 cells transfected with mutant receptor cDNAs were evaluated in radioligand binding and cyclic AMP assays. The CB_1 mutant and WT receptors were also co-expressed with G-protein-coupled inwardly rectifying channels (GIRK1 and GIRK4) in *Xenopus* oocytes to assess functional coupling. The Y → F mutation resulted in cannnabinoid receptors with subtle differences in WT binding and signal transduction. In contrast, the Y → I mutations produced receptors that could not produce signal transduction or bind to multiple cannabinoid compounds. However, immunofluorescence data indicate that the Y → I mutation was compartmentalized and expressed at a level similar to that of the WT cannabinoid receptor. These results underscore the importance of aromaticity at position CB_1 5.39(275) and CB_2 5.39(191) for ligand recognition in the cannabinoid receptors.

Keywords: Cannabinoid receptor; Mutation; Molecular model; Monte Carlo/Stochastic Dynamics; cAMP; Potassium currents

1. Introduction

The human CB_1 and CB_2 cannabinoid receptors, both G-protein-coupled receptors, share only 44% amino acid identity overall, with 68% identity within the transmembrane domains [1,2]. Most CB ligands, however, do not discriminate between the receptor subtypes [3,4] (reviewed in Refs. [5–7]). Both CB_1 and CB_2 receptors inhibit adenylyl cyclase activity via a pertussis toxin-sensitive G-protein [3,8,9]. In neuronal and transfected cells, the potency for inhibiting cAMP accumulation for a series of CB_1 receptor agonists correlates with their ability to displace CB binding [3,8]. The CB_1 receptor has also been shown to inhibit G-protein-coupled calcium and potassium channels [10,11].

There is growing evidence in the literature that the TMH 3-4-5 region is important for agonist/antagonist binding at both CB receptors. Shire *et al.* [12] reported that the TMH 4–5 region of CB_1 was crucial for high-affinity binding of the CB_1 antagonist SR141716A. Subsequent studies revealed that the TMH 4-extracellular2-TMH 5 region of both CB receptors contained residues critical for the binding of the aminoalkylindole WIN 55,212-2 and the CB_2 antagonist SR144528 [13]. Previous studies using the

* Corresponding author. Tel.: +1-415-923-3607; fax: +1-415-563-7325.
E-mail address: mabood@cooper.cpmc.org (M.E. Abood).

Abbreviations: CB, cannabinoid; cAMP, cyclic AMP; TMH, transmembrane helix; MC/SD, Monte Carlo/Stochastic Dynamics; WT, wild type; GIRK, G-protein-coupled inwardly rectifying potassium chanel; THC, tetrahydrocannabinol; GPCR, G-protein-coupled receptor.

0006-2952/02/$ – see front matter
PII: S0006-2952(02)01031-6

receptor model reported here identified an aromatic cluster in the TMH 3-4-5 region of both CB_1 and CB_2 as important to the binding of WIN 55,212-2 [14]. The CB_2 selectivity of WIN 55,212-2 was attributed to an additional direct interaction in CB_2 with F5.46(197), a residue that is non-aromatic in CB_1. These results led to the hypothesis that ligand interaction with F5.46(197) may be responsible for the CB_2 selectivity of WIN 55,212-2, and results of mutagenesis studies supported this hypothesis [14].

At the top of the TMH 3-4-5 aromatic cluster in both the CB_1 Y5.39(275) and CB_2 Y5.39(191) receptors is a tyrosine residue. Although our recent modeling studies have not identified Y275 or Y191 as a direct ligand interaction site [14,15], these studies have suggested that this residue may be a key element of the TMH 3-4-5 aromatic cluster in the CB receptors [16].

To test computationally if aromaticity or hydrogen bonding potential at position 5.39 was essential in the CB receptors, we used the MC/SD method, one that permits the simultaneous exploration of many thermally accessible conformational states of the receptor [17]. The MC/SD method was applied to WT CB_1 and to two mutant receptors, Y5.39(275)F and Y5.39(275)I. The first mutation preserves bulk and aromaticity at position 5.39, and tests if any hydrogen bonding potential is important at this position. The second mutation preserves bulk and tests if aromaticity is important. MC/SD results reported here show that the CB_1 Y275F mutant is very close to the WT, while results for the Y275I mutant show pronounced topology changes in the TMH 3-4-5 region. Furthermore, a detailed comparison of the CB model with the recently published 2.8 Å resolution crystal structure of rhodopsin [18] is included to highlight important similarities and differences.

Mutagenesis experiments were undertaken to test the effects of the 5.39 mutations in both the CB_1 and CB_2 receptors. Our strategy was to compare selective conservative mutations in both receptors rather than to study multiple less conservative mutations (e.g. alanines) in a single receptor. This strategy is based on our previous findings demonstrating that certain conserved amino acids among CB receptors are subtype-selective and play different roles in receptor function [15]. Here we report that the Y → F mutation in both CB_1 and CB_2 resulted in subtle alterations in receptor affinity and signal transduction. In contrast, the Y → I mutation in CB_1 and CB_2 led to receptors that lost ligand binding capability. Evaluation of receptor expression revealed no significant differences between the Y → I mutation and the WT receptor. Our MC/SD studies support the hypothesis that aromaticity at position 5.39(275) in CB_1 and 5.39(191) in CB_2 is essential to maintain cannabinoid ligand WT affinity.

2. Materials and methods

2.1. Molecular modeling

2.1.1. Amino acid number system

The numbering scheme suggested by Ballesteros and coworkers [19,20] was employed here. In this scheme, each amino acid position in a sequence is given a number that begins with the helix number followed by a two-digit decimal. The most highly conserved residue among GPCRs in each TMH is assigned a value of 0.50, and all other residues in the helix are numbered relative to this highly conserved residue. This numbering scheme is illustrated for CB_1 in Fig. 1, and a complete discussion of

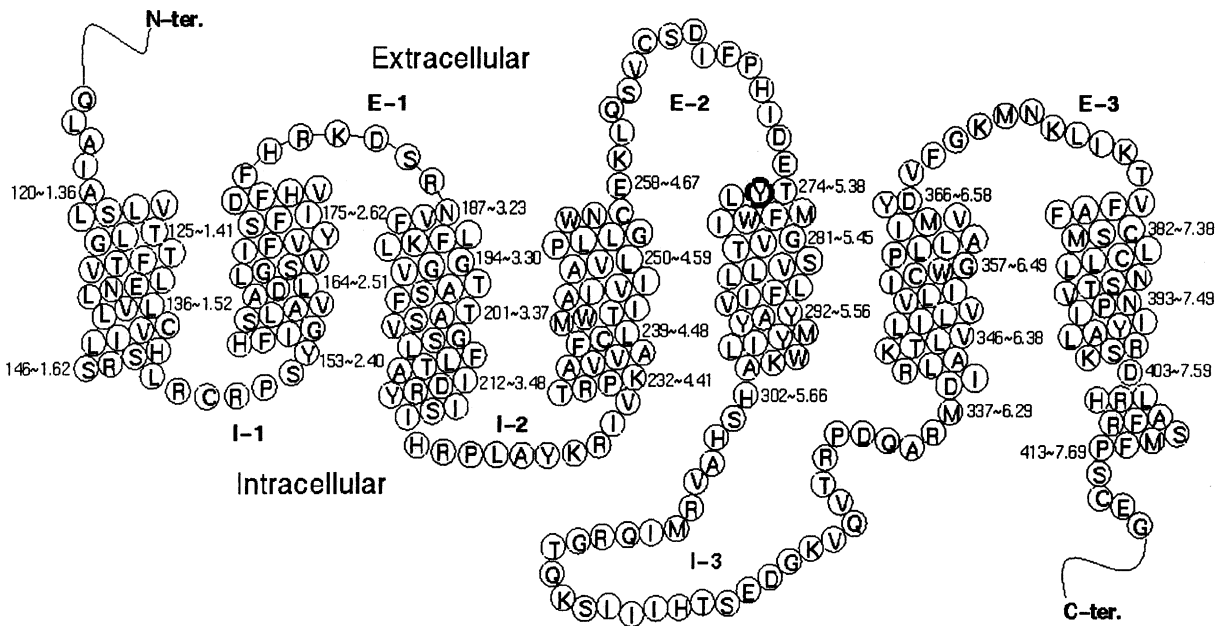

Fig. 1. Helix net representation of the sequence of the human CB_1 receptor.

sequence notation assignments can be found in an earlier publication [20].

It should be noted that TMH 5 of the CB receptors lacks the highly conserved Pro that is typically used to number residues in TMH 5 by this system. As detailed in an earlier paper [20], the second most highly conserved residue in TMH 5 of most GPCRs is a Tyr at position 5.58 in the C terminal portion of Hx 5. The CB_1 and CB_2 receptors have two Tyr residues in common in this region. To determine which of these would correspond to Tyr 5.58 in other GPCRs, a ''structural alignment'' was performed [19]. In such an alignment, residues are aligned based upon their predicted interior or surface-exposed character. First, the cytoplasmic end of TMH 5 was predicted using the criterion that Arg/Lys patches at the intracellular end of a TMH face the lipid domain and may serve to anchor the helix in the membrane by interaction with the negatively charged phospholipid head groups [21]. The cytoplasmic end of TMH 5 predicted using the Arg/Lys criterion was used then to superimpose the predicted accessibility profile for TMH 5 of CB_1 with the equivalent profile of the rest of the proteins used in the original alignment (see Ref. [20]). By this method, Y294 in CB_1 and Y210 in CB_2 were aligned with the highly conserved Tyr at 5.58 in other GPCRs. The Leu residue eight residues earlier in the sequence, normally a Pro, was assigned the locant 5.50 in order to preserve the numbering system corresponding to other GPCRs.

2.1.2. Computer model construction and refinement

The CB_1 TMH bundle model used as a starting structure for the MC/SD studies was constructed and refined as described previously [14] with three modifications. First, the initial conformation of TMH 7 was as obtained by Konvicka *et al.* [22], via Conformational Memories calculations. With this new conformation of TMH 7 introduced into the CB_1 bundle, a hydrogen bond network was established that included D2.50/N7.49/N1.50 [23]. A similar network is described for the $5\text{-}HT_{2a}$ receptor by Konvicka *et al.* [22]. Second, the conformation of TMH 6 used in the TMH bundle was obtained from a Conformational Memories [24] study of TMH 6 in CB_1. The conformation chosen reflected the kink produced by the CWXP motif in TMH 6 [25]. Finally, near the intracellular side of the TMH helix bundle, R3.50 was positioned to interact with D3.49 as described in Ballesteros *et al.* [26]. In this position, R3.50 can also form a salt bridge with D6.30. Such an interaction brings the intracellular ends of TMHs 3 and 6 in closer proximity, as has been suggested by Gether *et al.* [27] for the inactive state of the β_2-adrenergic receptor.

2.1.3. Model minimization

Residue 5.39 in WT CB_1 was mutated using MacroModel BatchMin (V5.5) [28] to either F or I. All calculations were performed using a distance-dependent dielectric. Each receptor bundle was packed before minimization using interactive computer graphics to maximize tertiary interactions between residue side chains. All of the WT, Y5.39F, and Y5.39I models were submitted to a minimization protocol using MacroModel BatchMin (V6.5). Before minimization, the charges on the following residue side chains were reduced to one-third the original value to prevent over-estimation of charge effects: E1.49, R1.61, D2.63, K3.28, R4.39, K4.41, K5.64, R6.32, K6.35, D6.58, R7.56, K7.58, and D7.59. Charges on these residues were reduced either because they face lipid or because they are not of functional importance. Residues D2.50, D3.49, R3.50, and D6.30 were left fully charged because these residues have been shown to be important to maintaining the receptor bundle in its inactive state [26].

The receptor model was minimized through a series of 11 cycles of 1000 iterations each. The first cycle consisted of Polak-Ribier conjugate gradient minimization with harmonic constraints on the backbone atoms. The output structure was then submitted to the second cycle of iterations in which the force constant on the helical backbone was reduced by 10%. Each subsequent cycle of iteration was computed with a further reduced force constant until the last cycle of iterations in which no constraints were placed on the backbone atoms.

2.1.4. MC/SD calculations

The MC/SD technique as described in Laakkonen *et al.* [17] was used here to study the effect of mutating Y5.39 to an F or to an I in the CB_1 receptor. This technique has been used successfully to explore the thermally accessible conformational states of the TRH receptor with its ligand, TRH [17]. The algorithm combines Stochastic Dynamics (SD) in Cartesian space with Metropolis Monte Carlo (MC) sampling in torsional space. In this method, after every dynamics step, a random trial torsional deformation is performed and accepted or rejected according to the Metropolis criterion. Regardless of the outcome of the Metropolis test, the next step is computed from the current conformation using the dynamical step to produce a new trial configuration of the Monte Carlo sampling. The mixed mode MC/SD calculation actually merges the algorithms of dynamics and Monte Carlo, essentially eliminating the distinction between deterministic and Stochastic simulations.

2.1.5. Stochastic dynamics heating

Each final minimized bundle was submitted to a Stochastic Dynamics heating protocol. Using MacroModel BatchMin 5.5, the receptor model was heated from 300 to 600 K in 25-degree increments. Each temperature was simulated for 25 psec using a time-step of 1.5 fsec. The simulation at 600 K ran for 100 psec, and 25 structures were sampled along the dynamical trajectory. A distance-dependent dielectric was used, and no constraints were applied.

2.1.6. MC/SD cooling

During the WT MC/SD cooling runs, χ_1 and χ_2 of the following residues were varied: F3.25, L3.29, F3.36, F3.44, Y3.51, F4.46, W4.50, W4.64, Y5.39, F5.42, W5.43, F5.53, Y5.56, Y5.60, C6.47, and W6.48. In addition, χ_1, χ_2, χ_3, and χ_4 of K3.28 were varied. β-Branched amino acids (V, I, and T) that are part of an α-helix have a single χ_1 population due to clashes with the helix backbone [29]. As a result, during the cool runs only χ_2 of the following β-branched residues was varied: I3.48, T5.47, and I6.46. Because T5.38 is the last residue at the top of Helix 5, it will not have limitations placed on its χ_1 value, so for T5.38 both χ_1 and χ_2 were varied. The torsion angles varied for the Y5.39F and Y5.39I mutants were the same as described above except at position 5.39. For the Y5.39F mutant, χ_1 and χ_2 of F5.39 were varied. For the Y5.39I mutant, χ_1 and χ_2 of I5.39 were varied.

The structures from the heating protocol were submitted to individual cooling runs using different random number seeds. For this protocol, the structures were cooled from 600 to 310 K using the MC/SD technique and the cooling scheme described below. The structure was cooled from 600 to 450 K in 25-degree increments, from 450 to 350 K in 20-degree increments, and from 350 to 310 K in 10-degree increments. Each of the first temperatures was simulated for 25 psec, using a time-step of 1.5 fsec. For each temperature, there was a 1:1 ratio of Monte Carlo to Stochastic Dynamics steps. At each MC step, 1 to 3 torsions from the list of possible torsion angles above were varied between $\pm 60^\circ$. The MacroModel adaptive mechanism for MC/SD calculations, which is a MacroModel default setting, was turned off using a system flag. At 310 K, the bundles were simulated for 50 psec, and 10 structures were sampled along the trajectory. Thus, there were 250 structures per each bundle system used for data analysis.

Centroids were created for each aromatic ring of each aromatic amino acid residue that faced into the CB_1 binding site crevice. These residues were F1.45, Y2.40, F2.42, F2.57, Y2.59, F2.61, F2.64, F2.67, F3.25, F3.27, F3.36, F3.44, Y3.51, F4.46, W4.50, W4.64, Y5.39 (F5.39 in the Y5.39F mutant), F5.42, W5.43, F5.53, Y5.56, Y5.58, Y5.60, W5.63, W6.48, Y6.57, F7.35, F7.37, and Y7.53 in WT CB_1. A vector normal to the plane of each aromatic system was also generated. The distances between centroids and the angle between the normal vectors, α, were measured for all possible pairs of aromatic amino acids within the TMH bundle. For each of the measurements described above, the average and standard deviation for each 250 bundle set were also computed. Burley and Petsko [30] have reported that aromatic–aromatic stacking interactions in proteins operate at distances (d) of 4.5 to 7.0 Å between ring centroids. The angle between normal vectors of interacting aromatic rings typically is between 30° and 90°, producing a "tilted-T" or "edge-to-face" arrangement of interacting rings. Residues were designated as part of a cluster if they had centroid to centroid distances between 4.5 and 7.0 Å. These interactions were further classified as "tilted-t" arrangements if $30^\circ \leq \alpha \leq 90^\circ$ and as parallel arrangements for $\alpha < 30^\circ$.

2.2. Mutation studies

2.2.1. Materials

[^{3}H]CP-55,940 ([^{3}H]-(−)-3-[2-hydroxyl-4-(1,1-dimethylheptyl)-phenyl]-4-[3-hydroxypropyl]cyclohexan-1-ol) was purchased from DuPont-NEN. Δ^9-THC and SR141716A [*N*-(piperidin-1-yl)-5-(4-chlorophenyl)-1-(2,4-dichlorophenyl)-4-methyl-1*H*-pyrazole-3-carboxamidehydrochloride] were obtained from the National Institutes on Drug Abuse. CP-55,940 was obtained from Pfizer Inc. WIN 55,212-2 [(*R*)-(+)-[2,3-dihydro-5-methyl-3-[(4-morpholinyl)methyl]pyrolo[1,2,3-*de*]-1,4-benzoxazin-6-yl](1-naphthalenyl)methanone] was purchased from RBI. Anandamide was synthesized and provided by Dr. Raj Razdan (Organix, Inc.). JWH-015 (2-methyl-3-napthoyl-*N*-propylindole) and JWH-051 (1-deoxy-11-hydroxy-Δ^8-THC-dimethylheptyl) were synthesized and provided by Dr. John Huffman (Clemson University). The human CB_1 cDNA clone was a gift of Dr. Marc Parmentier. Dr. Sean Munro (MRC Laboratories) provided the human CB_2 cDNA clone. GIRK1 and GIRK4 cDNA clones were a gift from Dr. Diomedes E. Logothetis.

2.2.2. Mutagenesis

Mutations were introduced with the QuikChange site-directed mutagenesis kit (Stratagene) as previously described [15]. This method allows mutagenesis to be performed in any vector; hence, we used human CB_1 or CB_2 subcloned into pcDNA3 (Invitrogen) [4]. The DNAs were sequenced to confirm mutation in the desired regions only. To make the CB_1 Y5.39F (Y275F) mutation, the primers C ATT GAT GAA ACC T**T**C CTG A TG TTC TGG (forward) and CCA GAA CAT CAG G**A**A GGT TTC ATC AAT G (reverse) containing the desired mutation (TAC to T**T**C) were used. The CB_2 Y5.39F (Y191F) mutation was made with the following primer sets: CCC AAT GAC T**T**C CTG CTG AGC TGG (forward) and CCA GCT CAG CAG G**A**A GTC ATT GGG (reverse). To make the Y5.39I (Y275I and Y191I) mutations, similar primers were constructed except that they contained the isoleucine mutation (TAC to A**T**C).

2.2.3. Cell culture and transfection

Cell lines were created by transfection of WT or mutant CB_1 or CB_2 pcDNA3 into HEK 293 cells by the Lipofectamine reagent as previously described [15]. Two or more cell lines containing moderate to high levels of receptor mRNA were tested for receptor binding and signal transduction properties. Each cell line had similar properties, so one was chosen for further analysis.

2.2.4. CB receptor radioligand binding determinations

The current assay has been described previously [31,32]. Briefly, cells were harvested in phosphate-buffered saline

containing 1 mM EDTA and centrifuged at 500 *g* (3 min, 22°). The cell pellet was homogenized and centrifuged three times at 1600 *g* (10 min, 4°). The combined supernatants were centrifuged at 100,000 *g* (60 min, 4°). The (P2 membrane) pellet was resuspended in 3 mL of buffer B (50 mM Tris–HCl, 1 mM EDTA, 3 mM $MgCl_2$, pH 7.4) to yield a protein concentration of approximately 1 mg/mL. Binding was initiated by the addition of 25–75 μg of membrane protein to silanized tubes containing [^{3}H]CP-55,940 (102.9 Ci/mmol) and a sufficient volume of buffer C (50 mM Tris–HCl, 1 mM EDTA, 3 mM $MgCl_2$, and 5 mg/mL of fatty acid-free BSA, pH 7.4) to bring the total volume to 0.5 mL. The addition of 1 μM unlabeled CP-55,940 was used to assess nonspecific binding. Specific binding averaged >50% of total binding in all cell lines used in the analysis. Following incubation (30° for 1 hr), binding was terminated by the addition of 2 mL of ice-cold buffer D (50 mM Tris–HCl, pH 7.4, plus 1 mg/mL of BSA) and rapid vacuum filtration through Whatman GF/C filters [pretreated with polyethyleneimine (0.1%) for at least 2 hr]. CP-55,940 and all cannabinoid analogs were prepared by suspension in assay buffer from a 1 mg/mL ethanolic stock without evaporation of the ethanol (final concentration of no more than 0.4%). When anandamide was used as a displacing ligand, experiments were performed in the presence of phenylmethylsulfonyl fluoride (50 μM). Saturation experiments were conducted with six concentrations of [^{3}H]CP-55,940 ranging from 250 pM to 10 nM. Competition assays were conducted with 0.5 nM [^{3}H]CP-55,940 and six concentrations (0.1 nM to 10 μM) of displacing ligands. Displacement EC_{50} values were originally determined by unweighted least-squares non-linear regression of log concentration–percent displacement data and then converted to K_i values using the method of Cheng and Prusoff [33] and re-analyzed with GraphPad Prism (GraphPad).

2.2.5. cAMP accumulation assay

Intracellular cAMP levels were measured with a competitive protein binding assay (Diagnostic Products, Inc.) as previously described [32]. Cells were harvested and resuspended at a concentration of 1×10^6 cells/mL in Dulbecco's modified Eagle's medium containing 20 mM HEPES, pH 7.3, 0.1 mM Ro-20-1724, and 1 mM isobutylmethylxanthine and incubated for 30 min at 37°. Aliquots of cells (90 μL) were added to polypropylene microfuge tubes containing 0.5 μM forskolin ± cannabinoids + 1 mg/mL of fatty acid-free BSA, in a final volume of 100 μL and incubated for 5 min at 37°. Since the cannabinoids were dissolved in ethanol, all tubes contained an equivalent amount of ethanol (0.5%). The reactions were terminated by boiling for 4 min, followed by centrifugation (12,000 *g*) and removal of 50 μL of the supernatant that was assayed for cAMP levels. The assay method is based on the competition between unlabeled cAMP and a fixed quantity of [^{3}H]cAMP for binding to a protein that has a high specificity and affinity for cAMP [34]. The amount of labeled cAMP protein complex formed is inversely related to the amount of unlabeled cAMP present in the assay sample. The free cAMP was separated from bound by adsorption onto dextran-coated charcoal, and the bound [^{3}H]cAMP was counted in a liquid scintillation counter. The concentration of cAMP in the unknown is determined by comparison with a linear standard curve. The results are expressed as percent inhibition of forskolin-stimulated cAMP accumulation. The EC_{50} curves were generated with the use of the GraphPad Prism program (GraphPad).

2.2.6. cRNA synthesis

cDNAs of GIRK1 and GIRK4 in pGEM-HE and CB_1, CB_1 Y275F, or CB_1 Y275I in pcDNA were linearized by *Nhe*I and *Xba*I, respectively. The cRNAs were transcribed *in vitro* using a T7 RNA polymerase (mMESSAGE mMACHINE, Ambion).

2.2.7. Expression in oocytes and recordings

Oocyte injection, expression, and recordings were performed as previously described [11]. Briefly, 0.1 to 0.3 ng of GIRK1 and GIRK4 and 14–25 ng of CB_1 (WT or mutant) cRNAs were co-injected using a micromanipulator (Drummond Scientific Co.) into *Xenopus laevis* oocytes. Recordings were performed after 7–9 days of incubation in 0.5× L-15 medium (Sigma) supplemented with L-glutamine and antibiotics. For recordings, the eggs were placed in a chamber (total volume 200 mL) and perfused at 4 mL/min with LK (2 mM KCl, 96 mM NaCl, 2 mM $CaCl_2$, 1.8 mM $MgCl_2$, and 5 mM HEPES, pH 7.5), HK (96 mM KCl, 2 mM NaCl, 2 mM $CaCl_2$, 1.8 mM $MgCl_2$, and 5 mM HEPES, pH 7.5), or HK plus drug. BSA (3 μM) was added to all drug solutions to minimize absorption of CB compounds to the perfusion system. Oocytes were impaled with two microelectrodes filled with 3 M KCl and were voltage-clamped at reported voltages using an Axon GeneClamp amplifier (Axon Instruments). Currents were filtered at 10 Hz, collected, and analyzed using a Macintosh Centris 650 containing a 16-bit analog-digital interface board and voltage-clamp software running under the IGOR graphics environment (Wavemetrics). The EC_{50} curves were generated with the use of the GraphPad Prism program (GraphPad).

2.2.8. Statistical analyses

The K_i and EC_{50} values in the mutant versus WT cell lines and oocytes were compared by analysis of logged data (GraphPad Prism) using the unpaired Student's *t*-test. *P* values <0.05 defined statistical significance.

2.2.9. Immunofluorescence

Immunocytochemical analyses were performed as previously described [15]. Briefly, cells seeded onto glass coverslips were fixed in 4% paraformaldehyde in PBS, and

then were treated with 0.01% Triton X-100 in PBS. Fixed coverslip cultures were blocked in SuperBlock (Pierce) in PBS, and incubated with an affinity-purified rabbit antibody (3 μg/mL in Superblock) directed against an immunodominant carboxy terminal domain of the human CB_1 receptor. This antibody, designated anti-hCB_1 417-438, was elicited in New Zealand White rabbits using a keyhole limpet hemocyanin-human CB_1 peptide (amino acids 417-438) fusion as immunogen and was assessed for specificity and antibody titer as described previously [35]. Following incubation with fluorescein isothiocyanate (FITC)-labeled goat anti-rabbit IgG, slides were mounted and examined with an Olympus BHA Microscope equipped with a model BH2RFl reflected fluorescence attachment and a model PM-10AD photo-micrographic system (Olympus Corp.). Percent fluorescence was determined following assessment of 100 cell profiles from each of four random fields. Positive fluorescence was defined as a positive/negative (*P*/*N*) ratio exceeding 2.1 based on comparison of fluorescence for a given cell versus that of the average of 100 untransfected cells incubated with preimmunization antibody and analyzed using SigmaScan software (SPSS Science). Controls consisted of cells transfected with the WT CB_1 receptor or with Y5.39(275)I receptor incubated with preimmunization serum obtained from the same rabbit, which was used to generate the anti-hCB_1 antibody. An additional control consisted of HEK 293 untransfected cells incubated with the anti-hCB_1 antibody.

3. Results

3.1. Molecular modeling

Fig. 1 illustrates the residue numbering system used in the modeling studies of CB_1. Molecular modeling studies were undertaken to develop structural hypotheses regarding the likely effects of the mutations. The MC/SD method was chosen because it has been shown previously to provide good sampling of the conformational space of a complex similar to the ones studied here, i.e. the TRH receptor [17]. One central interest in the work reported here was the aromatic stacking present in the CB_1 WT and mutant TMH bundles, because aromatic stacking has been shown to be important to ligand binding in the CB_1 and CB_2 receptors [14] and because the residue studied [Y5.39(275)] is itself an aromatic residue. The MC/SD method is capable of revealing alternate arrangements possible between aromatic residues in a TMH bundle because large changes in torsion angles can be taken during the MC steps. These large changes in torsion angle values permit the simulation to jump over energy barriers that might not be overcome by a simple simulated annealing protocol.

The acceptance rates for each cooling simulation were reasonable. For the WT simulation, these ranged from 14.61% at 600 K to 6.85% at 310 K. For the Y5.39(275)F mutant, the acceptance rates were 14.23% at 600 K and 6.78% at 310 K, while for the Y5.39(275)I mutants they were 15.06 and 7.30%, respectively. In all simulations, the total energy changed in a parallel fashion with temperature throughout the cooling phase.

The CB receptor TMH bundles studied here are comprised of seven independent helices without connecting extracellular or intracellular loops. The environment of the bundle, i.e. the phospholipid membrane, has been simulated by a simple distance-dependent dielectric. It has been shown previously for the TRH receptor that the additional kinetic energy at the elevated temperatures used in the MC/SD protocol did not result in the dissociation of the receptor bundle model, a model comprised of seven independent helices with an identical treatment of the environment [17]. We found that the bundles held together well during the simulations reported here.

3.2. Analysis of MC/SD results

The MC/SD method was used here largely to reveal an overall picture of the alternative sets of interactions that might be possible in each bundle and the relative probability of these arrangements. The centroid to centroid distance criterion proposed by Burley and Petsko [30] for aromatic stacking interactions was used as a way to screen multiple bundles for the proximity of rings to each other and the identification of cluster patterns of aromatic residues. We examined the effects of mutation of Y5.39 to phenylalanine (F) or isoleucine (I). The first mutation resulted in a loss of a hydrogen bonding moiety, but retention of aromaticity and bulk. The second mutation resulted in loss of aromaticity, but preservation of hydrophobic bulk.

For each run [i.e. WT, Y5.39(275)F, and Y5.39(275)I], the resultant set of 250 bundles was analyzed for degree of helicity as determined by the number of backbone hydrogen bonds maintained between residues i and $i + 4$ in each helix. We found that the bundles after cooling retained between 60 and 70% helicity with TMHs 3 (58%) and 7 (50%) below this range, due presumably to the NPXXY motif inTMH 7 [22] and the presence of two adjacent glycine residues in TMH 3 [G3.30(194)/G3.31(195)] that are exposed to lipid. As might be expected, non-systematic unwinding of helix ends was observed in some of the bundles. Laakkonen *et al.* [17] also reported some unwinding of helices at each end in their MC/SD study of the TRH/TRH receptor complex. Because of this unwinding in some of the CB_1 bundles, one concern was the position of residue 5.39 as it is near the extracellular end of TMH 5. When this unwinding occurred at the top of TMH 5 during the simulations, the first turn of TMH 5 looped over the binding site crevice. In their substituted cysteine accessibility studies of the dopamine D2 receptor, Javitch *et al.* [36] reported that 10 consecutive residues [F5.38(189) to

F5.47(198)] at the top of TMH 5 were accessible from within the binding site crevice. The authors suggested that this pattern of exposure is inconsistent with the idea that TMH 5 forms a fixed α-helix in this region; instead, this region of TMH 5 might loop out into the lumen of the binding site crevice and be completely accessible to water and to the methanethiosulfonate ethylammonium reagent used in substituted cysteine accessibility studies. Thus, the unwinding seen at the top of TMH 5 in some of the MC/SD runs reported here should not confound interpretation of results.

The integrity of the D3.49(213)/R3.50(214)/D6.30(338) complex salt bridge in each bundle was also analyzed. In their analysis of 94 proteins from the Protein Data Bank, Musafia *et al.* [37] defined interactions between Lys/Arg and Asp/Glu with N to O distances ≤4 Å to be salt bridges. Consequently, a 4-Å cut-off was used here to screen for salt-bridge interactions in each set of bundles. In greater than 90% of the WT, Y5.39(275)F, and Y5.39(275)I bundles, the complex salt bridge involving D3.49(213)/R3.50(214)/D6.30(338) remained intact.

Although the majority of interacting aromatic rings in the CB_1 bundle for each receptor system were in "tilted-t" arrangements where $30° \leq \alpha \leq 90°$ [30], we did identify some off-set parallel arrangements where $0° < \alpha < 30°$ [38]. For example, nine Y5.56(292)/F5.53(289) stacking interactions were classified as parallel, while 134 interactions were classified as "tilted-t."

The upper half of the binding site crevice towards the extracellular space is a region where small ligand binding is commonly thought to occur in GPCRs. Our major focus was on the extracellular half of the TMH 3-4-5-6 region because this region has been implicated in the binding of several CB_1 agonists/antagonists [12–14] and shown to be important for receptor activation in other GPCRs [27]. The following pairs of residues met the centroid distance criterion in the WT bundle (the numbers in brackets are the number of bundles in which a pair was identified): F3.36(200)/W5.43(279) {113}, F3.36(200)/W6.48(356) {136}, Y5.39(275)/W5.43(279) {140}, W4.64(255)/Y5.39(275) {98}, and W4.64(255)/F5.42(278) {62}. In the Y5.39(275)F mutant, F3.36(200)/W5.43(279) {132}, F3.36(200)/W6.48(356) {156}, F5.39(275)/W5.43(279) {170}, and W4.64(255)/F5.39(275) {69} met the centroid distance criterion. In the Y5.39(275)I mutant, F3.36(200)/W5.43(279) {199} and W5.43(279)/W6.48(356) {145} met the criterion.

Results for the extracellular half of the bundle described above reveal that the WT and Y5.39(275)F bundles were similar in the identity of aromatic residues involved in clusters. However, the frequencies of these interactions were not the same for the WT and Y5.39(275)F bundles, indicating subtle differences between these two receptors.

Data analysis of the WT and mutant receptor models consistently showed two major structural differences between the WT and Y5.39(275)F bundles versus the Y5.39(275)I bundle. The first difference involves the ligand binding pocket and arrangement of key residues. The second major difference is the loss of an aromatic stacking interaction between W4.64(255) and Y5.39(275) at the top of TMHs 4 and 5.

3.2.1. The F3.36(200)/W5.43(279)/W6.48(356) triad

In the ligand binding pocket, three residues consisting of F3.36(200), W5.43(279), and W6.48(356) are consistently involved in aromatic stacking interactions in the WT and mutant receptor TMH bundles. However, as seen in Figs. 2 and 3, the arrangement of this triad is significantly different in the Y5.39(275)I mutant. In the WT bundle (Fig. 2), residue F3.36(200) acts as a communication link between W5.43(279) and W6.48(356). W5.43(279) and W6.48(356) rarely interact directly with each other. Results for the Y5.39(275)F bundle were similar to those for WT. In the Ile mutant, however, W5.43(279) now appears to link F3.36(200) and W6.48(356) through indirect stacking interactions, as seen in Fig. 3; now F3.36(200) and W6.48(356) rarely interact via direct aromatic stacking interactions. The positioning of W5.43(279) between F3.36(200) and W6.48(356) actually forces a change in the χ_1 angle preference for both residues. For F3.36(200), the g^+ and trans χ_1 conformations are nearly equally populated in the WT CB_1 bundles. However, the χ_1 population shifts towards g^+ (76%) in the Y5.39(275)I mutant. Residue 6.48(356) prefers g^+ and trans nearly equally in the WT, but is now predominantly g^+ (85%) in the Y5.39(275)I mutant.

3.2.2. The W4.64(255)—Y5.39(275) stack

In the WT receptor, there is a dominant interaction via an aromatic stack between residues W4.64(255) and Y5.39(275). When the aromaticity of 5.39 is lost, as in the isoleucine mutant, this interaction between TMH 4 and 5 at the extracellular end is lost. To compensate, W4.64(255) repositions itself to stack with other hydrophobic residues in the bundle. As a result of the loss of this key interaction between TMH 4 and 5, the extracellular end of TMH 5 moves further into the binding site crevice producing a rearrangement of interactions described above for the F3.36(200)/W5.43(279)/W6.48(356) triad. It is important to note, however, that as described above for the intracellular and extracellular halves of the binding site crevice, the CB_1 TMH bundle of the Y5.39(275)I mutant adjusts to the loss of aromaticity at 5.39 by establishing new interactions. Therefore, the modeling results indicate that the TMH bundle of the Y5.39(275)I mutant should be stable.

3.3. Comparison of the CB model with rhodopsin

Palczewski *et al.* [18] recently published a 2.8 Å resolution crystal structure of bovine rhodopsin (Rho) that contains 11-*cis*-retinal covalently linked to Rho through Lys 296. This structure represents the inactive (R) conformation of Rho. Both the CB receptors and Rho belong to the

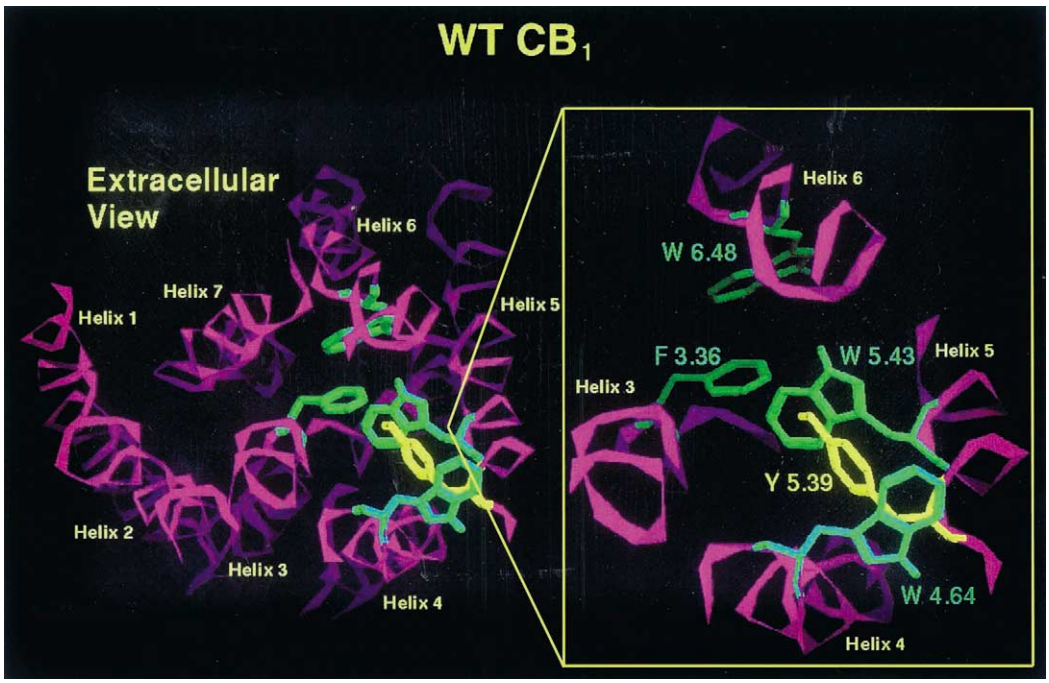

Fig. 2. Aromatic stacking interactions in the TMH 3-4-5-6 region for WT CB_1. Tyr 5.39 (yellow) is part of an aromatic cluster that includes W4.64, W5.43, F3.36, and W6.48 (all shown in green).

same sub-family of GPCRs. It can therefore be expected that the 2.8 Å Rho structure and the CB_1/CB_2 receptors will bear many structural similarities. This should be particularly true at the intracellular ends of these receptors, as all function in the same way: by coupling to G-protein located intracellularly. The similarities in the primary sequence of these receptors are evident in the pattern of conserved motifs, such as the (E/D)RY motif in TMH 3, the CWXP motif in TMH 6, and the NPXXY motif in TMH 7 of both the CB receptors and Rho and in other highly

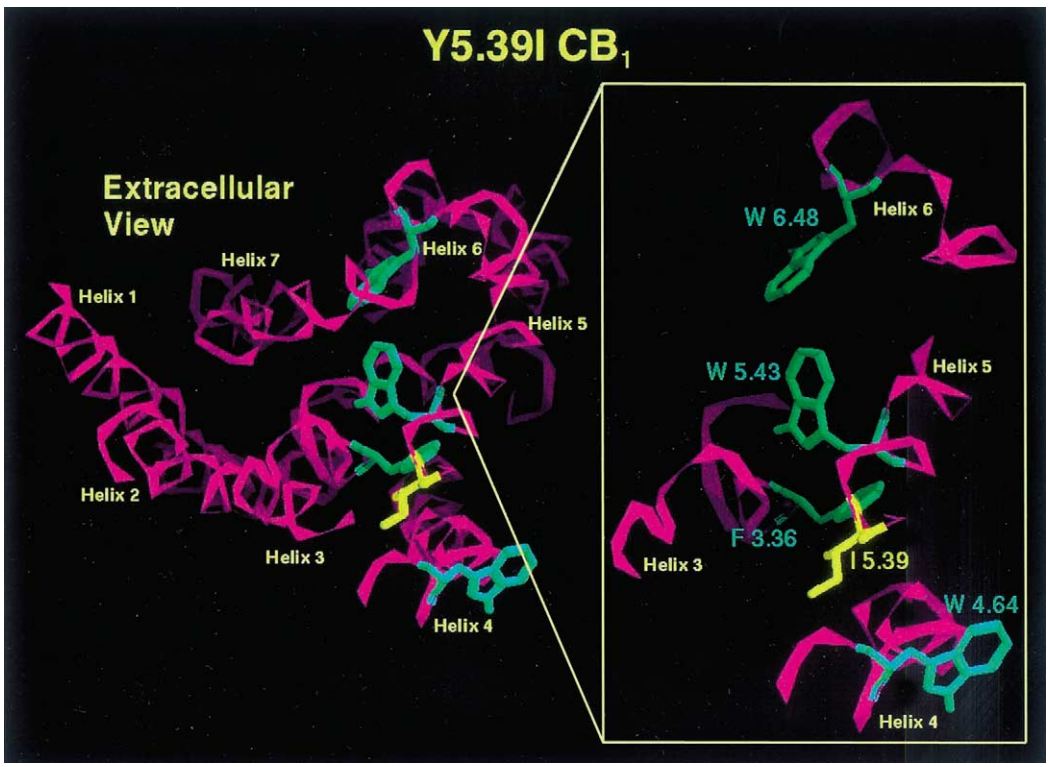

Fig. 3. Aromatic stacking interactions in the TMH 3-4-5-6 region for the Y5.39I CB_1 mutant. The loss of aromaticity at 5.39 (now Ile5.39, shown in yellow) has produced a re-arrangement in the TMH 3-4-5-6 region such that W6.48/W5.43/F3.36 alone stack, but in a different arrangement than in WT (Fig. 2).

conserved single amino acids such as Asn 1.50 in TMH 1, Asp 2.50 in TMH 2, and Trp 4.50 in TMH 4.

Ligand specificity among GPCRs arises from receptor sequence divergences, particularly towards the extracellular ends of TMH bundles, as this region is thought to form the binding site crevice for small ligands such as the classical CBs. When this region of the GPCR sequences differs in proline content or the occurrence of GG motifs, TMH conformations can be expected to diverge in these regions somewhat from the Rho structure. There are several divergences from Rho apparent in the CB sequences on the extracellular side. These include the absence of helix kinking residues in TMH 1 [P1.48 (53) in Rho, but L1.48 in CB_1 and CB_2], as well as the lack of a GG motif [G2.56(89), G2.57(90) in Rho; but I2.56(169), F2.57(170) in CB_1; V2.56(86), F2.57(87) in CB_2]. In CB_1, there is a GG motif in TMH 3 [G3.31(194), G3.32(195)] close to the extracellular end that is exposed to lipid. This motif can be expected to create a region of flexibility/kink in TMH 3 of CB_1, by analogy to the TMH 2 GG motif in Rho. Such flexibility was seen in the MC/SD studies presented here. Rhodopsin contains a Pro residue at position 5.50(215) in TMH 5. This Pro residue does not cause a large kink in TMH 5, but does cause an increase in the phi and psi backbone torsion angles in TMH 5 above this residue. The result is a shift in the position of all residues extracellular to the Pro. The CB receptors lack this Pro and therefore will exhibit a more normal alpha helical TMH conformation in this region. A final important difference between Rho and the CB receptors is a key disulfide bridge. In Rho, a TMH 3 residue Cys3.25(110) is engaged in a disulfide bridge with a Cys residue in the E2 loop. The 2.8 Å structure of Rho shows that this causes the E2 loop to dip down in the binding site crevice above (extracellular to) 11-*cis*-retinal. There is no corresponding Cys residue in TMH 3 of the CB receptors. However, there is a Cys residue at the extracellular end of TMH 4 and a Cys near the middle of the E2 loop in the CB receptors. Recent mutation results [39] for CB_2 suggest that a bridge between these two Cys residues (C174, C179) may exist, but further work is needed to prove the existence of this bridge. As the result of this important difference between Rho and the CB receptors, the binding site crevice around TMHs 3-4-5 is likely to be different.

With these anticipated similarities and differences, we compared the 2.8 Å Rho structure with the CB_1 models developed previous to the publication of the Rho structure. As detailed in a previous paper (see Ref. [14] and references therein), the model used in this paper was constructed using a convergence of methods that relied on sequence similarities between GPCRs, on photo-affinity labeling, spin-labeling, NMR, mutation, scanning cysteine accessibility, metal ion cross-linking, electron microscopy, and other studies of GPCRs. As a result of the large amount of experimental information that went into the construction of the CB_1 model, it is not surprising that the CB_1 TMH bundle used here compared very well to the 2.8 Å structure of the Rho TMH bundle. Fig. 4 illustrates that the Rho and

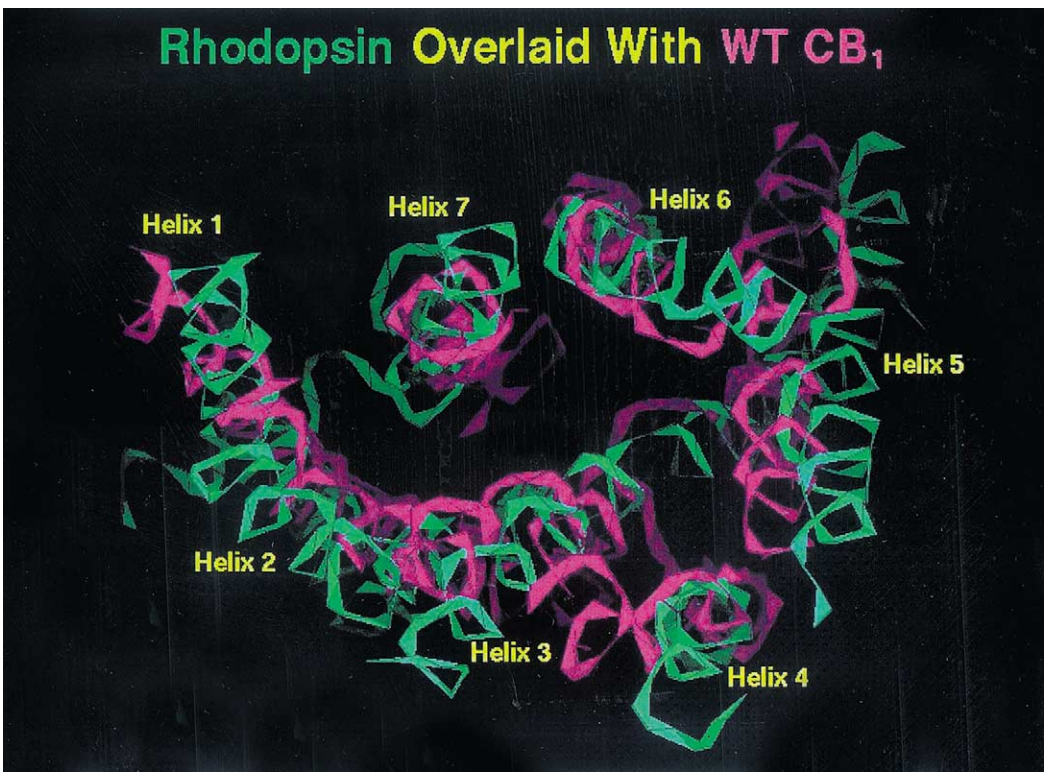

Fig. 4. Extracellular view of an overlay of the transmembrane (TM) domains of the 2.8 Å structure of bovine rhodopsin [18] with the TM domains of WT CB_1 as calculated using the MC/SD method.

WT CB_1 TMH bundles are similar in helix tilts and helix packing. On the intracellular side of the bundle, the Rho structure shows an important interaction between E3.49/R3.50/E6.30, an interaction that has been proposed to function as an "ionic lock" in the β_2-adrenergic receptor, constraining the intracellular ends of TMHs 3 and 6 in the inactive state of this receptor [40]. As discussed above, an analogous interaction (D3.49/R3.50/D6.30) was found in over 90% of the CB_1 TMH bundles studied here. The position of Cys 6.47 in the TMH bundle is important as its position differs between the R and R^* states of GPCRs [41]. In Rho, which is in the R state, and in the CB_1 models, this Cys is located at the TMH 6-7 interface.

When the CB_1 model was constructed, experimental evidence was used to set the relative heights of TMHs 2, 3, 6, and 7 (see Ref. [14] and references therein). We found that the relative positions of these TMHs in the CB models agreed with those in Rho. For the other helices in the CB model, in the absence of experimental evidence, assumptions were made to position the other helices. For example, an underlying assumption was that the highly conserved N1.50 and D2.50 are at the same relative height and may interact with each other [23]. In the 2.8 Å Rho structure, N1.50 and D2.50 are at the same relative height; however, they do not interact directly.

When the CB_1 model was originally built, we used an analysis of the alpha periodicity in hydrophobicity and variability [20] in the sequences of CB_1, CB_2, and related receptors to delineate the helix ends and helix orientations. This method has an expected error of ± one turn on an alpha helix (i.e. ~3.6 residues). A comparison of TMH helix ends with Rho revealed that our designation of helix ends was indeed within one turn for six out of seven helices (see Fig. 1 for representation of helix ends used in the CB models). Only in TMH 1 was there a greater deviation from Rho. Here the N terminus of our TMH 1 began seven residues later than the N terminus in Rho and ended three residues past the end of TMH 1 in Rho. It is possible, due to sequence differences between Rho and the CB receptors, that our original assignment of TMH 1 ends was correct for the CB receptors, as this assignment was based on the hydrophobicity and sequence variability among receptors highly homologous to CB_1 (i.e. CB_2, MSH, ACTH, EDG-1, α-$_{1C}$-adrenergic and α-$_{1B}$-adrenergic receptors; see [20]). Alternatively, the Rho TMH 1 ends may be found in the CB receptors. In either case, what is most important to the TMH bundle is that the relative height of TMH 1 is correct. A comparison with the Rho structure reveals, as mentioned previously, that this residue in the CB models was placed at the same relative height as D2.50, a situation that is present in Rho.

It is very important to the work presented here that the relative heights of TMHs 3-5-6 be correct, as our studies implicated residues on these three TMHs as forming an important triad. Inspection of the Rho structure revealed that the relative heights of TMHs 3-5-6 in the CB_1 models were consistent with those in Rho. Finally, the MC/SD studies reported here showed frequent interaction between W4.64 and Y5.39 in WT CB_1 and between W4.64 and F5.39 in the Y5.39F mutant. This interaction may stabilize the relative positions of the extracellular ends of TMHs 4 and 5, as TMH 4 and 5 assume a very different relative position when there is no longer an aromatic residue at position 5.39 (i.e. as in the Y5.39I mutant). In the Rho crystal structure [18], a similar interaction involving W4.64 is evident. Here, W4.64(175), which is at the end of TMH 4 and the beginning of the E2 loop in Rho, is engaged in an aromatic stacking interaction with F203, a residue in a position equivalent to Y5.39 in the CB_1 bundle.

3.4. Mutation studies

To assess the role of the tyrosine residue in the fifth transmembrane domain (Y5.39) conserved between the CB_1 and CB_2 cannabinoid receptors (Y275 and Y191, respectively), we substituted a phenylalanine or an isoleucine. Stable cell lines were established that expressed the human CB_1, CB_2 (wild type), Y5.39I, or Y5.39F receptors in HEK 293 cells. The CB_1 receptor and mutant cRNAs were also expressed in *Xenopus* oocytes and assessed for coupling to co-expressed GIRK channels. The CB_2 receptor was not studied in *Xenopus* oocytes since this receptor does not couple efficiently to GIRK channels [11]. Ligand binding to the WT and mutant receptors was probed using four structurally distinct classes of CB agonists [the classical CBs (Δ^9-THC, JWH-051); non-classical cannabinoids (CP-55,940); indoles (WIN 55,212-2, JWH-015); and eicosanoids (anandamide)] and the CB_1 antagonist, SR141716A [7,42].

3.5. Ligand recognition in WT and mutant Y5.39 receptors

K_d and B_{max} values of 5.2 (2.9 to 7.5) nM and 2.3 (1.8 to 2.7) pmol/mg protein, respectively, were obtained using [^{3}H]CP-55,940 as a radioligand in the HEK 293 cell line expressing WT CB_1 (Table 1). In the cell line stably

Table 1
Scatchard analysis of WT and mutant cell lines

Cell line	K_d (nM)	B_{max} (pmol/mg)
CB_1	5.2 (2.9–7.5)	2.3 (1.8–2.7)
Y275F	4.7 (1.7–7.5)	3.5 (2.4–4.7)
Y275I	NSB	NSB
CB_2	0.60 (0.08–1.3)	2.1 (1.3–2.8)
Y191F	1.7 (0.08–3.6)	0.8 (0.5–1.7)
Y191I	NSB	NSB
HEK 293	NSB	NSB

Saturation experiments using [^{3}H]CP-55,940 were performed on stably transfected HBK 293 cells to evaluate binding affinities and relative levels of receptor expression in the WT and mutant receptors. Nonspecific binding was determined in the presence of excess CP-55,940 (see Section 2). Data are the means and corresponding 95% confidence limits of three independent experiments, each performed in triplicate. NSB, no specific binding.

Table 2
Binding profile of WT and mutant Y5.39F cell lines

Ligand	CB_1 K_i/K_d (nM)	Y275F K_i/K_d (nM)	CB_2 K_i/K_d (nM)	Y191F K_i/K_d (nM)
Δ^9-THC	37 (14–93)	9.8 (1.3–69)	33 (14–98)	8.7 (1.0–73)
Anandamide	450 (188–1076)	6155* (877–24230)	188 (48–736)	4623* (1161–12870)
WIN 55,212-2	1.3 (0.4–2.2)	7.8 (1.7–14.0)	1.0 (0.5–1.5)	3.6 (1.3–6.0)
SR141716A	7.1 (1.8–27)	15 (8.1–27)	ND	ND
JWH-015	ND	ND	89 (61–131)	147 (21–1024)
JWH-051	ND	ND	0.38 (0.28–0.53)	0.25 (0.04–1.5)

Inhibition constants were obtained from competition experiments using stably transfected HEK 293 cells (see Section 2). Data are the means and corresponding 95% confidence limits of three independent experiments, each performed in triplicate. ND, not determined.
* Statistically significant differ from WT ($P < 0.05$).

expressing the CB_2 receptor, K_d and B_{max} values of 0.60 (0.08 to 1.3) nM and 2.1 (1.3 to 2.8) pmol/mg protein were obtained (Table 1). As previously reported [4,15], Hill coefficients did not deviate from 1.0 in these experiments, indicating a single binding site.

The K_d and B_{max} values obtained for the Y5.39F mutant receptors (Y275F and Y191F, Table 1) were not significantly different from WT receptors. In contrast, the Y5.39I mutant cell lines did not show any specific binding with [^{3}H]CP-55,940 (Y275I and Y191I, Table 1) or [^{3}H]SR141716A (data not shown). No specific [^{3}H]CP-55,940 binding to HEK 293 cells was found prior to transfection (data not shown).

To characterize the pharmacological profile of the mutant receptors, several representative CB compounds were compared in competition binding assays (Table 2). As shown in Table 2, the phenylalanine mutant receptors had reduced affinity for anandamide compared to WT.

3.6. Signal transduction properties of WT and mutant Y5.39 receptors

The ability of the mutant receptors to activate second messenger systems was evaluated. In accordance with the binding data, the Y5.39F mutant receptor-expressing cell lines showed concentration-responsive CP-55,940- and WIN 55,212-2-mediated inhibition of forskolin-stimulated cAMP accumulation, similar to that of WT expressing cells (Fig. 5, A–D).

The EC_{50} values with the corresponding 95% confidence limits were 4.3 (2.8 to 6.7) nM for WIN 55,212-2 and 5.8 (2.6 to 13) nM for CP-55,940 in the WT CB_1 cells, with E_{max} values of 38 (36 to 41) and 39 (34 to 43) % forskolin stimulation (maximal inhibition of 62%) (Table 3). The EC_{50} values were 7.9 (1.2 to 53) nM for WIN 55,212-2 and 19 (9.4 to 39) nM for CP-55,940 for the WT CB_2-293 cells, with E_{max} values of 61 (48 to 73) and 56 (52 to 62) % forskolin stimulation (maximal inhibition of 43%) (Table 3). The EC_{50} values were 16 (1.2 to 23) nM for WIN 55,212-2 and 141.1 (24 to 820) nM for CP-55,940 in the CB_1 Y5.39(275)F cells, with E_{max} values of 62 (53 to 71) and 59 (52 to 66) % forskolin stimulation (maximal inhibition of 38%). The EC_{50} values were 4.8 (0.28 to 84) nM for WIN 55,212-2 and 10 (0.6 to 170) nM for CP-55,940 for the WT CB_2 Y5.39(191)F cell line, with E_{max} values of 53 (40 to 66) and 48 (30 to 65) % forskolin stimulation (maximal inhibition of 52%) (Table 3). The levels of forskolin-stimulated cAMP accumulation in the absence of added CB compounds did not vary significantly between the WT and the mutant cell lines (Fig. 5).

In contrast to the phenylalanine mutations, the Y5.39I mutations resulted in alterations in signaling responses. No concentration-responsive inhibition of forskolin-stimulated cAMP accumulation was observed with either WIN 55,212-2 or CP-55,940 (Fig. 5, A–D).

To assess whether the defect in receptor activation in the Y5.39I mutation was limited to G-proteins associated with adenylyl cyclase activity, the ability of the CB_1 Y5.39(275) receptors to activate inwardly rectifying potassium channels in *Xenopus* oocytes was determined. Co-expression of WT CB_1 receptors with a G-protein-coupled inwardly rectifying potassium channel (GIRK1 and GIRK4 subunits) resulted in a concentration-dependent enhancement of the potassium current (Fig. 6), as previously demonstrated [11,43]. Furthermore, co-injection of Y5.39(275)F with GIRK1/4 resulted in expression of a receptor with proper-

Table 3
Comparison of potencies for inhibition of intracellular cAMP accumulation in WT and mutant cell lines

Agonist	Cell line	EC_{50} (nM)	E_{max} (% forskolin stimulation)
WIN 55,212-2	CB_1	4.3 (2.8–6.7)	38 (36–40)
	Y275F	16 (1.2–22)	62 (53–71)
	Y275I		82 (66–98)
	CB_2	7.9 (1.2–54)	61 (49–74)
	Y191F	4.8 (0.28–84)	53 (40–67)
	Y191I		77 (55–101)
CP-55,940	CB_1	5.8 (2.6–13)	39 (34–43)
	Y275F	141 (24.2–820)*	59 (52–66)*
	Y275I		91 (86–98)
	CB_2	19 (9.4–40)	57 (52–62)
	Y191F	10 (0.6–170)	48 (30–65)
	Y191I		100 (95–105)

Data are the means and corresponding 95% confidence limits of three independent experiments, each performed in triplicate.
* Statistically significant differences from WT ($P < 0.05$).

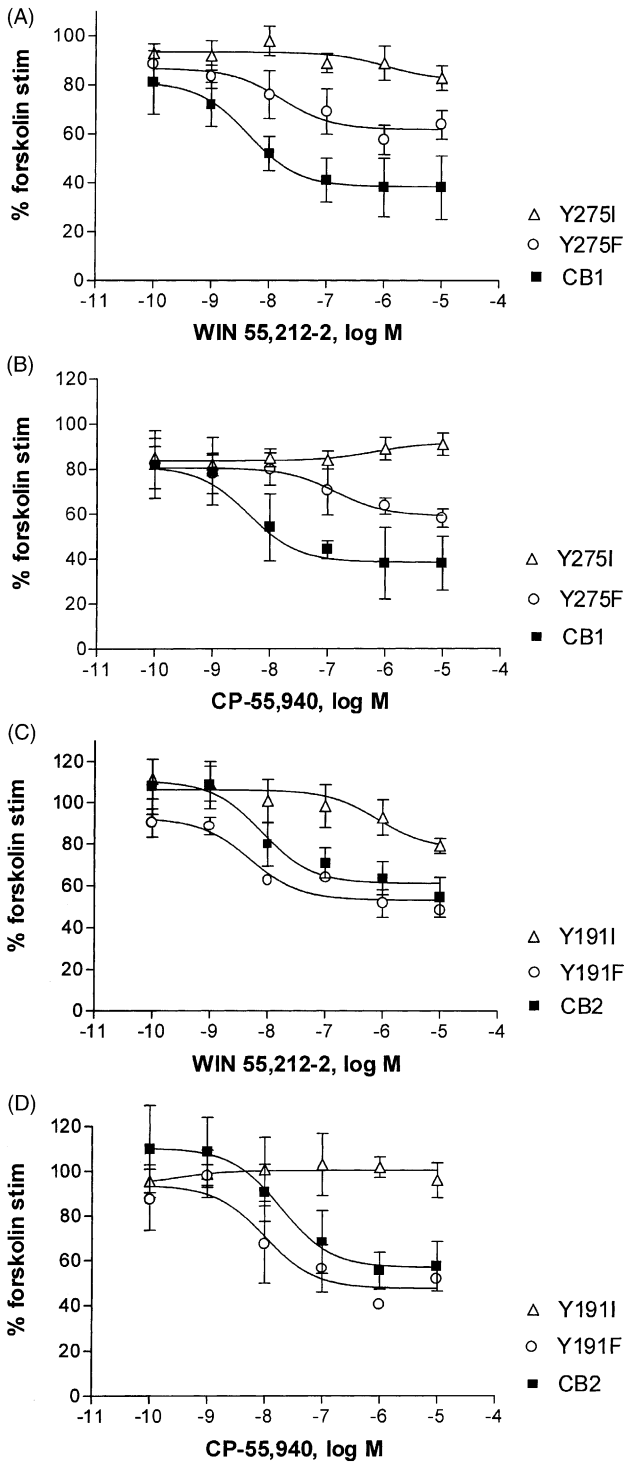

Fig. 5. Comparison between the WT and the mutant CB_1 and CB_2 receptors for agonist-induced inhibition of cAMP accumulation by WIN 55,212-2 (A and C) or CP-55,940 (B and D). cAMP accumulation assays were performed on HEK 293 cells stably expressing WT CB_1 (■) or Y275I (△) or Y275F (○) mutant receptor cDNAs (A and B) or wild type CB_2 (■) or Y191I (△) or Y191F (○) mutant receptor cDNAs (C and D). Each point is the mean ± SEM of three or more independent experiments performed in triplicate. Curves were generated as described in Section 2. Levels of basal and forskolin-stimulated cAMP accumulation (expressed in pmol/10^6 cells/min), respectively, for the cell lines tested were: CB_1: 2.22 ± 0.53, 5.78 ± 0.93; Y275F: 1.37 ± 0.11, 7.01 ± 0.22; Y275I: 3.09 ± 0.89, 6.34 ± 0.64; CB_2: 1.32 ± 0.19, 5.46 ± 0.65; Y191F: 1.00 ± 0.29, 6.17 ± 0.48; and Y191I: 1.15 ± 0.12, 4.35 ± 0.31.

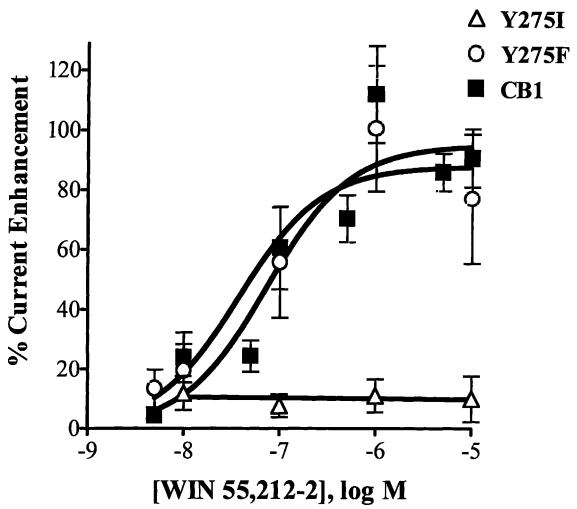

Fig. 6. Concentration–response analysis in oocytes co-expressing GIRK1/4 and WT or mutant CB_1 cRNAs. Oocytes were co-injected with 0.1 to 0.3 ng of GIRK1/4 and 0.1 to 0.3 ng of CB_1 (■), Y275F (○), or Y275I (△) cRNAs. Each data point in the concentration–response curve is the mean ± SEM of at least four determinations made from two batches of oocytes. Recordings were performed as described in Section 2.

ties similar to those of WT CB_1 (Fig. 6). The potencies of WIN 55,212-2 and the maximum current enhancement produced by Y5.39(275)F expressing oocytes were not significantly different from CB_1 expressing oocytes. Values with the corresponding 95% confidence intervals for Y275F/GIRK1/4 were 37 nM (8–170) and E_{max} = 88% (60–116), and for CB_1/GIRK1/4, EC_{50} = 73 nM (24–219) and E_{max} = 95% (76–114). However, no enhancement of current was observed in oocytes co-injected with Y5.39(275)I and GIRK1/4 (Fig. 6).

3.7. Immunofluorescence studies

Immunofluorescence studies were performed using an antibody directed against an immunodominant carboxy terminal domain of the human CB_1 receptor in order to define the cellular localization of the expressed mutant Y5.39(275)I proteins. Although the cell lines examined were clonal in origin, differences in shape and size were observed in the cultures. Representative photomicrographs are shown in panels A–C of Fig. 7.

Approximately 90% of cells transfected with the WT CB_1 receptor were positive for fluorescence (Fig. 7A). A diffuse, as well as a punctate or studded "dot" distribution, pattern of immunofluorescence was observed. Approximately 10% of the cells exhibited a punctate pattern of immunofluorescence in the cytoplasm. The majority of the cells exhibited diffuse cytoplasmic staining and concentrated staining delineating the outer margin of the cytoplasm (Fig. 7). This latter staining pattern is consistent with localization of the recombinant receptor on the cell surface. Cells expressing the Y5.39(275)I receptor exhibited a staining pattern similar to that of the WT receptor (Fig. 7B). However, there was an increase in the number

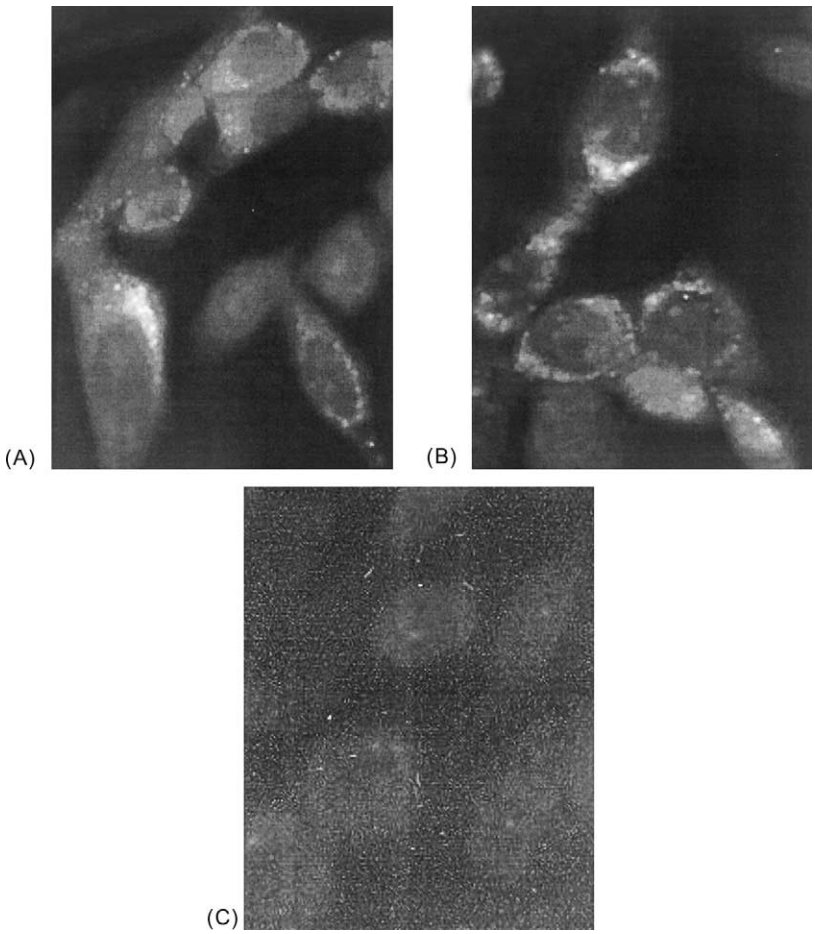

Fig. 7. Immunofluorescence staining of HEK 293 cells. (A) Cells expressing WT CB_1 receptors. (B) Cells transfected with Y275I mutant. (C) Untransfected HEK 293 cells reacted with anti-CB_1 417-438 antibody. (A–C, magnification 600×).

of cells exhibiting punctate immunofluorescence within the cytoplasm compared with the WT transfected cells (approximately 20 vs. 10%). Perinuclear staining could be observed in both HEK 293 cells expressing WT CB_1 receptor as well as Y5.39(275)I. Untransfected HEK 293 cells and transfected cells incubated with normal rabbit IgG exhibited minimal fluorescence (Fig. 7C). Thus, the immunofluorescence data indicate that Y5.39(275)I was expressed in a manner similar to that of the WT CB_1 receptor.

4. Discussion

The chemical nature of the conserved tyrosine residue in the fifth transmembrane domain of the CB_1 and CB_2 receptor is critically important to the recognition site of the CB receptors. In both the CB_1 and CB_2 receptors, mutation of tyrosine to phenylalanine resulted in receptor proteins with subtle changes in binding and signal transduction characteristics of the native receptor. In contrast, the tyrosine to isoleucine mutation resulted in a loss of ligand binding.

4.1. Molecular modeling

4.1.1. Aromatic clusters

In our computer models of the CB_1 and CB_2 receptor, residue 5.39 is near the extracellular end of Helix 5. The corresponding residue in TMH 5 has been shown to be available to the binding site crevice in the dopamine D2 receptor [36] and to form part of the binding site for antagonists in the rat μ opioid receptor [44]. In the CB models, residue 5.39 forms part of an aromatic cluster in the TMH 3-4-5-6 region. Aromatic clusters such as the CB_1/CB_2 TMH 3-4-5-6 cluster discussed in Section 3 (see Fig. 2) have been proposed to form the binding site of other GPCRs, including the TRH receptor [45] and the dopamine D2 receptor [46–48]. Previous receptor modeling studies have identified the TMH 3-4-5 region and residues F3.25, F3.36, W4.64, Y5.39, F5.42, and W5.43 (and F5.46 in CB_2) as the binding site for WIN 55,212-2 in the CB receptors, with F3.25, F3.36, and W5.43 (and F5.46 in CB_2) in direct interaction with the ligand [14]. Mutation studies at position 5.46 in CB_1 versus CB_2 have suggested that residue 5.46 is responsible for the CB_2 selectivity of WIN 55,212-2 [14]. CB chimera studies have pointed to

the TMH4-E2-TMH5 region of the CB receptor sequences as important to the binding of WIN 55,212-2 and SR141716A in CB_1 and of SR144528 in CB_2 [13]. Our modeling studies have suggested that both SR antagonists interact in the TMH 3-4-5-6 region that is described here (unpublished studies).

4.1.2. Ligand binding in models of the Y5.39F, Y275F, and Y275I mutants

Modeling results reported here indicate that while the TMH bundles of the WT and the Y5.39F mutant are similar, a significant change in the CB_1 binding site crevice in the TMH 3-4-5-6 region results from the Y5.39I mutation. Presumably a similar change would occur in CB_2. Residues on TMHs 3, 5, 6, and 7 in CB_1 and TMHs 3, 6, and 7 in CB_2 have been proposed to be important to the binding of CP-55,940 [49]. Given that the binding site crevice undergoes a change in shape upon the mutation of Y5.39 to I because of the movement of TMH 5, it is not surprising that the WT binding site of CP-55,940 was also affected. No alternate binding site for CP-55,940 could be identified in the Y5.39I mutant models.

4.2. Ligand binding

4.2.1. Y → F mutants

The CB_1 Y5.39F and CB_2 Y5.39F mutations were made to test if hydrogen bonding is an important interaction at the 5.39 locus. In this case, a loss in affinity upon mutation to F would be expected. As revealed in Table 2, the binding of anandamide Y5.39(275)F was found to be statistically different from its CB_1 and CB_2 WT affinities. Anandamide showed a 12- and a 24-fold drop in affinity relative to CB_1 and CB_2 WT, respectively. Loss of affinity of these receptors for anandamide could possibly be attributed to the loss of a direct hydrogen bonding interaction. Fersht [50] has estimated that loss of such a hydrogen bond should cost between 1.5 and 1.8 kcal/mol. This would result in between a 12- and 20-fold diminishment in affinity.

4.2.2. Y → F mutants: functional characteristics

There were some subtle alterations in the functional characteristics of the CB_1 Y5.39(275)F mutant receptors. There was a slight reduction in the ability of the CB_1 Y275F receptor protein to inhibit cAMP accumulation. This result suggests that in the CB_1 receptor even a slight alteration of this residue is critical for proper receptor function. However, the CB_2 Y to F mutation had no effect on cAMP accumulation. We have previously identified differences in CB_1 and CB_2. Mutation of a conserved lysine to an alanine in the CB_1 (K192A) and CB_2 (K109A) receptor resulted in proteins with drastically different characteristics [15,51,52]. The K to A mutation dramatically altered CB_1 receptor function but had no effect on the CB_2 receptor. Modeling studies suggested that the CB_2 receptor could compensate for this mutation due to an interaction with a serine residue unique to CB_2 [15].

4.2.3. Y → I mutants

In contrast to the phenylalanine mutations, the tyrosine to isoleucine mutations resulted in loss of ligand recognition and function in both CB receptors. No specific binding of CP-55,940 was seen in the Y5.39I mutants. Signal transduction in the isoleucine mutant cell lines was also lost as assessed by receptor coupling to adenylyl cyclase or GIRK channels, respectively. However, we cannot rule out that the loss of activation is not due to the loss of ligand binding.

To address whether the loss of ligand recognition in the CB_1 Y5.39(275)I mutant receptor was due to incorrect processing and/or compartmentalization of the receptors, immunofluorescence studies were carried out using a CB_1 receptor antibody. Both cell lines exhibited a similar pattern of immunostaining. For a majority of the cells, staining was within the cytoplasmic compartment in a diffuse pattern and in some cases apparently delineating the outer periphery, suggesting receptor localization at the cell surface. A smaller percentage of cells also exhibited a punctate pattern of fluorescence. The punctate distribution of immunofluorescence is consistent with accumulation of receptor within vesicular structures, suggestive of vesicular transport of receptor from the perinucleus to the cell surface. The only exception was a slight increase in the number of CB_1 Y5.39(275)I mutant receptor cells exhibiting a punctate pattern of fluorescence in the cytoplasm. However, we did not consider this to represent a significant change in receptor expression and processing since in previous studies where we have seen incorrect processing and/or compartmentalization the staining patterns show entrapment of immunoreactive product within perinuclear regions and its absence at the periphery [15]. The immunofluorescence data suggest that the Y275I mutant receptor is properly expressed in the context of cellular distribution and localization and that the pattern of receptor distribution is similar to that of the WT receptor. In addition, the results from the immunofluorescence studies, while non−quantitative, indicate that expression of the Y5.39I mutant receptor occurred at levels sufficient for the performance of ligand binding. Standard immunofluorescence is a relatively insensitive method as compared with immunoenzyme approaches, and positive staining is indicative of levels of protein that should allow for assessment of ligand binding. Finally, intensity of cellular immunofluorescence, and the approximate numbers of positive cells within cultures, for the Y275I mutant receptor were comparable to those of the WT receptor for which membranes yielded high-affinity binding. Collectively, these results led us to conclude that alterations in ligand recognition are due to altered interactions within the binding site of the receptor protein as opposed to global structural perturbation in the protein.

Our molecular modeling studies suggested the critical nature of residue 5.39. Therefore, we used the strategy of preserving bulk at CB_1 and CB_2 5.39 by mutations to Y and I. Indeed, subsequent to reporting our initial preliminary findings at the CB_1 5.39 locus [53], Shire *et al.* [13] showed that the CB_1 receptor Y5.39(275)S and Y5.39(275)A mutations resulted in receptors that failed to be expressed on the cell surface. Unfortunately, when such receptor sequestration occurs, the only conclusion that can be drawn is that residue 5.39(275) may be an important global structural component of the receptor. In this paper, we show that the strategy of preserving bulk in both CB receptors helps demonstrate a more detailed role for this residue in ligand binding and receptor activation.

5. Conclusions

The substitution of phenylalanine for Y5.39 in both CB_1 and CB_2 resulted in changes in ligand binding affinities and normal signal transduction. The magnitude of change in ligand affinities was too small to be attributed to the loss of a hydrogen bonding interaction, but was more consistent with a slight alteration of inter-residue aromatic/hydrophobic interactions as suggested in the MC/SD results reported here. The substitution of isoleucine for Y5.39 produced receptors that could not recognize CB ligands. This alteration did not appear to be the result of improper expression of the mutant receptor in the context of cellular distribution and localization. Taken together, these results are consistent with the hypothesis that aromaticity at position 5.39 is important for normal ligand binding in both CB_1 and CB_2 receptors. Modeling results suggest that the loss of aromaticity, but the preservation of hydrophobic bulk at position 5.39 changes the global position of TMH 5 and the arrangement of aromatic residues in the W5.43/F3.36/W6.48 triad. Such changes lead to a disruption of the normal stacking involved in the ligand binding pocket.

Acknowledgments

This work was supported by National Institutes of Health Grants DA-09978 and DA05274 (to M.E.A.) and DA-03934 (to P.H.R.).

References

[1] Gerard CM, Mollereau C, Vassart G, Parmentier M. Molecular cloning of a human cannabinoid receptor which is also expressed in testis. Biochem J 1991;279:129–34.
[2] Munro S, Thomas KL, Abu-Shaar M. Molecular characterization of a peripheral receptor for cannabinoids. Nature 1993;365:61–5.
[3] Felder CC, Joyce KE, Briley EM, Mansouri J, Mackie K, Blond O, Lai Y, Ma AL, Mitchell RL. Comparison of the pharmacology and signal transduction of the human cannabinoid CB_1 and CB_2 receptors. Mol Pharmacol 1995;48:443–50.
[4] Showalter VM, Compton DR, Martin BR, Abood ME. Evaluation of binding in a transfected cell line expressing a peripheral cannabinoid receptor (CB_2): identification of cannabinoid receptor subtype-selective ligands. J Pharmacol Exp Ther 1996;278:989–99.
[5] Howlett AC. Pharmacology of cannabinoid receptors. Annu Rev Pharmacol Toxicol 1995;35:607–34.
[6] Pertwee RG. Pharmacology of cannabinoid CB_1 and CB_2 receptors. Pharmacol Ther 1997;74:129–80.
[7] Rinaldi-Carmona M, Barth F, Millan J, Derocq J-M, Casellas P, Congy C, Oustric D, Sarran M, Bouaboula M, Calandra B, Portier M, Shire D, Brelière J-C, Le Fur G. SR144528, the first potent and selective antagonist of the CB_2 cannabinoid receptor. J Pharmacol Exp Ther 1998;284:644–50.
[8] Howlett AC, Fleming RM. Cannabinoid inhibition of adenylate cyclase. Pharmacology of the response in neuroblastoma cell membranes. Mol Pharmacol 1984;26:532–8.
[9] Slipetz DM, O'Neill GP, Favreau L, Dufresne C, Gallant M, Gareau Y, Guay D, Labelle M, Metters KM. Activation of the human peripheral cannabinoid receptor results in inhibition of adenylyl cyclase. Mol Pharmacol 1995;48:352–61.
[10] Mackie K, Hille B. Cannabinoids inhibit N-type calcium channels in neuroblastoma-glioma cells. Proc Natl Acad Sci USA 1992;89:3825–9.
[11] McAllister SD, Griffin G, Satin LS, Abood ME. Cannabinoid receptors can activate and inhibit G-protein-coupled inwardly rectifying potassium channels in a *Xenopus* oocyte expression system. J Pharmacol Exp Ther 1999;291:618–26.
[12] Shire D, Calandra B, Delpech M, Dumont X, Kaghad M, Le Fur G, Caput D, Ferrara P. Structural features of the central cannabinoid CB_1 receptor involved in the binding of the specific CB_1 antagonist SR141716A. J Biol Chem 1996;271:6941–6.
[13] Shire D, Calandra B, Bouaboula M, Barth F, Rinaldi-Carmona M, Casellas P, Ferrara P. Cannabinoid receptor interactions with the antagonists SR141716A and SR144528. Life Sci 1999;65:627–35.
[14] Song ZH, Slowey C-A, Hurst DP, Reggio PH. The difference between the CB_1 and CB_2 cannabinoid receptors at position 5.46 is crucial for the selectivity of WIN 55212-2 for CB_2. Mol Pharmacol 1999;56:834–40.
[15] Tao Q, McAllister SD, Andreassi J, Nowell KW, Cabral GA, Hurst DP, Bachtel K, Ekman MC, Reggio PH, Abood ME. Role of a conserved lysine residue in the peripheral cannabinoid receptor (CB_2): evidence for subtype specificity. Mol Pharmacol 1999;55:605–13.
[16] Reggio P, Hurst D, Barnett-Norris J, Song Z, Tao Q, McAllister S, Abood M. Computational studies of Helix 5 residues of the CB receptors that are important for ligand interaction, subtype selectivity and activation. In: International Cannabinoid Research Society, editor. Symposium on the cannabinoids, Stone Mountain, GA, 1998. Burlington, VT: International Cannabinoid Research Society, 1998. p. 25.
[17] Laakkonen LJ, Guarnieri F, Perlman JH, Gershengorn MC, Osman R. A refined model of the thyrotropin-releasing hormone (TRH) receptor binding pocket. Novel mixed mode Monte Carlo/Stochastic Dynamics simulations of the complex between TRH and TRH receptor. Biochemistry 1996;35:7651–63.
[18] Palczewski K, Kumasaka T, Hori T, Behnke CA, Motoshima H, Fox BA, Le Trong I, Teller DC, Okada T, Stenkamp RE, Yamamoto M, Miyano M. Crystal structure of rhodopsin: a G-protein-coupled receptor. Science 2000;289:739–45.
[19] Ballesteros JA, Weinstein H. Integrated methods for the construction of three-dimensional models and computational probing of structure function relations in G-protein-coupled receptors. In: Conn PM, Sealfon SM, editors. Methods in neuroscience, vol. 25. San Diego: Academic Press, 1995. p. 366–428.
[20] Bramblett RD, Panu AM, Ballesteros JA, Reggio PH. Construction of a 3D model of the cannabinoid CB_1 receptor: determination of helix ends and helix orientation. Life Sci 1995;56:1971–82.
[21] Ballesteros JA, Weinstein H. Analysis and refinement of criteria for predicting the structure and relative orientations of transmembranal helical domains. Biophys J 1992;62:107–9.

[22] Konvicka K, Guarnieri F, Ballesteros J, Weinstein H. A proposed structure for transmembrane segment 7 of G-protein-coupled receptors incorporating an Asn-Pro/Asp-Pro motif. Biophys J 1998;75:601–11.
[23] Zhou W, Flanagan C, Ballasteros JA, Konvicka K, Davidson JS, Weinstein H, Millar RP, Sealfon SC. A reciprocal mutation supports Helix 2 and Helix 7 proximity in the gonadotropin-releasing hormone receptor. Mol Pharmacol 1994;45:165–70.
[24] Guarnieri F, Weinstein H. Conformational memories and the exploration of biologically relevant peptide conformations: an illustration for the gonadotropin-releasing hormone. J Am Chem Soc 1996;118: 5580–9.
[25] Barnett-Norris J, Hurst DP, Buehner K, Ballesteros JA, Guarnieri F, Reggio PH. Agonist alkyl tail interaction with cannabinoid CB_1 receptor V6.43/I6.46 groove induces a Helix 6 active conformation. Int J Quantum Chem 2002;88:76–86.
[26] Ballesteros J, Kitanovic S, Guarnieri F, Davies P, Fromme BJ, Konvicka K, Chi L, Millar RP, Davidson JS, Weinstein H, Sealfon SC. Functional microdomains in G-protein-coupled receptors. The conserved arginine-cage motif in the gonadotropin-releasing hormone receptor. J Biol Chem 1998;273:10445–53.
[27] Gether U, Lin S, Ghanouni P, Ballesteros JA, Weinstein H, Kobilka BK. Agonists induce conformational changes in transmembrane domains III and VI of the β_2 adrenoceptor. EMBO J 1997;16:6737–47.
[28] Mohamadi F, Richards N, Guida W, Liskamp R, Lipton M, Caulfield C, Chang G, Hendrickson T, Still W. MacroModel—an integrated software system for modeling organic and bioorganic molecules using molecular mechanics. J Comput Chem 1990;11:440–67.
[29] McGregor M, Islam S, Sternberg M. Analysis of the relationship between side-chain conformation and secondary structure in globular proteins. J Mol Biol 1987;198:295–310.
[30] Burley S, Petsko G. Aromatic–aromatic interaction: a mechanism of protein structure stabilization. Science 1985;229:23–8.
[31] Compton DR, Rice KC, De Costa BR, Razdan RK, Melvin LS, Johnson MR, Martin BR. Cannabinoid structure–activity relationships: correlation of receptor binding and *in vivo* activities. J Pharmacol Exp Ther 1993;265:218–26.
[32] Tao Q, Abood ME. Mutation of a highly conserved aspartate residue in the second transmembrane domain of the cannabinoid receptors, CB_1 and CB_2, disrupts G-protein coupling. J Pharmacol Exp Ther 1998;285:651–8.
[33] Cheng YC, Prusoff WH. Relationship between the inhibition constant (K_I) and the concentration of inhibitor which causes 50% inhibition (I_{50}) of an enzymatic reaction. Biochem Pharmacol 1973;22:3099–4108.
[34] Tovey KC, Oldham KG, Whelan JA. A simple direct assay for cyclic AMP in plasma and other biological samples using an improved competitive protein binding technique. Clin Chim Acta 1974;56: 221–34.
[35] Pettit DAD, Showalter VM, Abood ME, Cabral GA. Expression of a cannabinoid receptor in baculovirus infected insect cells. Biochem Pharmacol 1994;48:1231–43.
[36] Javitch JA, Fu D, Chen J. Residues in the fifth membrane-spanning segment of the dopamine D2 receptor exposed in the binding-site crevice. Biochemistry 1995;34:16433–9.
[37] Musafia B, Buchner V, Arad D. Complex salt bridges in proteins: statistical analysis of structure and function. J Mol Biol 1995;254:761–70.
[38] Hunter CA, Singh J, Thornton JM. π–π interactions: the geometry and energetics of phenylalanine–phenylalanine interactions in proteins. J Mol Biol 1991;218:837–46.
[39] Gouldson P, Calandra B, Legoux P, Kernéis A, Rinaldi-Carmona M, Barth F, Le Fur G, Ferrara P, Shire D. Mutational analysis and molecular modelling of the antagonist SR144528 binding site on the human cannabinoid CB_2 receptor. Eur J Pharmacol 2000;401:17–25.
[40] Ballesteros JA, Jensen AD, Liapakis G, Rasmussen SGF, Shi L, Gether U, Javitch JA. Activation of the β_2-adrenegic receptor involves disruption of an ionic lock between the cytoplasmic ends of transmembrane segments 3 and 6. J Biol Chem 2001;276: 29171–7.
[41] Javitch JA, Fu D, Liapakis G, Chen J. Constitutive activation of the β_2-adrenergic receptor alters the orientation of its sixth membrane-spanning segment. J Biol Chem 1997;272:18546–9.
[42] Rinaldi-Carmona M, Barth F, Heaulme M, Shire D, Calandra B, Congy C, Martinez S, Maruani J, Neliat G, Caput D, Ferrar P, Soubrie P, Breliere JC, Fur GL. SR141716A, a potent and selective antagonist of the brain cannabinoid receptor. FEBS Lett 1994;350:240–4.
[43] Henry DJ, Chavkin C. Activation of inwardly rectifying potassium channels (GIRK1) by co-expressed rat brain cannabinoid receptors in *Xenopus* oocytes. Neurosci Lett 1995;186:91–4.
[44] Chen C, Yin J, de Riel JK, DesJarlais RL, Raveglia LF, Zhu J, Liu-Chen L-Y. Determination of the amino acid residue involved in [^{3}H]β-funaltrexamine covalent binding in the cloned rat μ opioid receptor. J Biol Chem 1996;271:21422–9.
[45] Colson A, Perlman J, Jinsi-Parimoo A, Nussenzveig D, Osman R, Gershengorn M. A hydrophobic cluster between transmembrane Helices 5 and 6 constrains the thyrotropin-releasing hormone receptor in an inactive conformation. Mol Pharmacol 1998;54:968–78.
[46] Javitch JA, Ballesteros JA, Weinstein H, Chen J. A cluster of aromatic residues in the sixth membrane-spanning segment of the dopamine D2 receptor is accessible in the binding-site crevice. Biochemistry 1998;37:998–1006.
[47] Javitch JA, Ballesteros JA, Chen J, Chiappa V, Simpson MM. Electrostatic and aromatic microdomains within the binding-site crevice of the D2 receptor: contributions of the second membrane-spanning segment. Biochemistry 1999;38:7961–8.
[48] Simpson MM, Ballesteros JA, Chiappa V, Chen J, Suehiro M, Hartman DS, Godel T, Snyder LA, Sakmar TP, Javitch JA. Dopamine D4/D2 receptor selectivity is determined by a divergent aromatic microdomain contained within the second, third, and seventh membrane-spanning segments. Mol Pharmacol 1999;56:1116–26.
[49] Reggio P. Ligand–ligand and ligand–receptor approaches to modeling the cannabinoid CB_1 and CB_2 receptors: achievements and challenges. Curr Med Chem 1999;8:665–83.
[50] Fersht AR. Relationships between apparent binding energies measured in site-directed mutagenesis experiments and energetics of binding and catalysis. Biochemistry 1988;27:1577–80.
[51] Song Z-H, Bonner TI. A lysine residue of the cannabinoid receptor is critical for receptor recognition by several agonists but not WIN 55212-2. Mol Pharmacol 1996;49:891–6.
[52] Chin CN, Lucas-Lenard J, Abadji V, Kendall D. Ligand binding and modulation of cyclic AMP levels depend on the chemical nature of residue 192 of the human cannabinoid receptor 1. J Neurochem 1998;70:366–73.
[53] Abood M, Tao Q, McAllister S, Hurst D, Reggio P. A critical role for a tyrosine residue in the cannabinoid receptors for recognition of several compounds excluding indoles. In: International Cannabinoid Research Society, editor. Symposium on the cannabinoids, Stone Mountain, GA, 1998. Burlington, VT: International Cannabinoid Research Society, 1998. p. 24.